Ultrafast dynamics of photoinduced semiconductor-to-metal transition in the optical switching nano-oxide Ti_3O_5

Akifumi Asahara,[1] Hiroshi Watanabe,[1] Hiroko Tokoro,[2,3] Shin-ichi Ohkoshi,[2] and Tohru Suemoto[1]
[1]*Institute for Solid State Physics, University of Tokyo, 5-1-5 Kashiwanoha, Kashiwa, Chiba 277-8581, Japan*
[2]*Department of Chemistry, School of Science, University of Tokyo, 7-3-1 Hongo, Bunkyo-ku, Tokyo 113-0033, Japan*
[3]*Division of Materials Science, Faculty of Pure and Applied Sciences, University of Tsukuba, 1-1-1 Tennodai, Tsukuba, Ibaraki 305-8573, Japan*

(Received 30 April 2014; revised manuscript received 27 June 2014; published 14 July 2014)

Nanogranular trititanium pentaoxide (Ti_3O_5), an oxide showing a photoreversible phase transition at room temperature, has recently attracted considerable attention because of its applicability in optical data storage. We report the dynamics of the photoinduced semiconductor-to-metal transition (β phase to λ phase) at room temperature. With time-resolved diffuse reflection spectroscopy conducted over a wide range of time scales, from femtoseconds to microseconds, the overall relaxation behavior was characterized. We found that a transient phase transition occurs within a few hundreds of femtoseconds and that 40% of the converted λ-phase fractions revert to β phase within 1 ps. Carriers are generated instantaneously and disappear within 20 ns. The λ phase increases from 1 to 10 ps, indicating growth of the metallic domain. A slow recovery process, with a duration ranging from 10^{-9} to 10^{-4} s, was found and is ascribed to the shrinking and annihilation of the size-distributed metastable λ-phase domains. The fast onset, with a duration within a few hundreds of femtoseconds and the subsequent stabilization process of less than 10 ps, signal the applicability of this material to ultrafast photoswitching.

DOI: 10.1103/PhysRevB.90.014303 PACS number(s): 71.30.+h, 82.50.Hp, 78.47.jb, 72.80.Ga

I. INTRODUCTION

Optical control of the electronic, magnetic, and optical properties of solids via photoinduced phase transitions [1] has recently been of great interest in materials science and technology. Ultrafast switching phenomena have various applications, which utilize the drastic and permanent changes in physical properties within ultrafast time scales, caused by photoinduced phase transitions. These features are particularly applicable directly to high-density and quickly rewritable optical data storage techniques. To date, many types of photoinduced phase transitions have been discovered, such as order-disorder phase transitions in chalcogenides [2,3], insulator-metal transitions in metal oxides [4–6], neutral-ionic phase transitions in organic compounds [7,8], spin-crossover transitions in metal complexes [9,10], and photomagnetism in cyano-bridged assemblies [11–14]. In relation with the development of these materials, their properties and optical responses have been studied in order to understand their underlying mechanisms and improve their functionality. Based on this background, we focus on nanogranular trititanium pentaoxide (Ti_3O_5) [15–18], which was developed recently and has been attracting considerable attention as a photofunctional material. In general, titanium oxides are a fascinating functional material group because they exhibit the occurrences of various types of phase transitions or optical responses depending on stoichiometric ratios, e.g., TiO_2 [19], Ti_2O_3 [20,21], or Ti_4O_7 [22–24]. In addition, since the element Ti is nontoxic and economical, this family of materials is highly anticipated for their sustainability as functional materials.

Ti_3O_5 has been known to exhibit temperature-induced metal-semiconductor transitions, and this property has been studied in electrical, thermodynamic, and crystallographic investigations [15,16,25–32]. The transition temperature lies in the vicinity of 460 K, and the metallic phase (α phase) is stable at higher temperatures, while the semiconductor phase (β phase) is stable at lower temperatures, including room temperature. The crystal structures of the α and β phases are orthorhombic ($Cmcm$) and monoclinic ($C2/m$), respectively. The semiconductor β phase has a band gap of about 0.14 eV. In the β phase, the valence states for the three nonequivalent Ti ions in the unit cell are close to Ti^{3+}-$Ti^{11/3+}$-$Ti^{10/3+}$. This means that the β phase has a form of charge ordering and the carriers are localized, resulting in semiconductorlike conductivity.

Recently, in nanogranular Ti_3O_5, a metallic λ phase at room temperature has been discovered [15]. Although this phase cannot exist in macroscopic crystals, it is thermodynamically stable due to nanoscale size effects. The λ phase has a monoclinic structure and belongs to the space group $C2/m$, which is the same as that of the β phase. However, it differs in that the lattice constant along the c axis for the λ phase is about 5% larger than that for the β phase. In the λ phase, every Ti ion has a valence state close to $Ti^{10/3+}$ and less charge-density fluctuation occurs, resulting in a carrier-delocalized system. This electronic structure is similar to that of the metallic α phase, while the crystal symmetry is different.

In addition, it has been reported that the β phase and the λ phase can be switched, reversibly, by optical excitation [15]. This was the first demonstration of a photoreversible oxide at room temperature. Hence, nanogranular Ti_3O_5 has attracted considerable attention as a material for high-density rewritable optical storage. From the perspective of thermodynamics, this switching phenomenon is interpreted as a photoinduced phase transition between the truly stable β phase and the metastable λ phase, which is a thermodynamically trapped state at a local energy minimum.

This photoinduced phase transition has the further unique characteristic that the direction of the transition can be controlled by simply adjusting the excitation fluence at a constant wavelength. When increasing the irradiation fluence, a sample in the β phase is transferred to the λ phase when the fluence

passes a threshold. When the λ phase is irradiated at a fluence several times larger than this threshold, the λ phase reverts to the β phase. Although this fluence-dependent reversibility is interesting, the mechanism remains unclear. In order to understand such a complicated phenomenon, the relaxation dynamics following the optical stimulation must be studied. In this report we focus on the photoinduced semiconductor-to-metal phase transition (β phase to λ phase) and investigate the relaxation dynamics through time-resolved diffuse reflection spectroscopy. By observing the phenomena over a wide range of time scales, from femtoseconds to microseconds, the entire relaxation behavior was characterized.

II. EXPERIMENT

We prepared a pellet of β-Ti_3O_5 with diameter 6 mm and thickness ∼1 mm. The β-Ti_3O_5 powder was prepared via a pressure-induced phase transition from λ-Ti_3O_5 flakes consisting of aggregated nanoparticles (25 ± 15 nm), synthesized by sintering anatase-TiO_2 particles in a hydrogen atmosphere [15]. The pellets' conversion to β-Ti_3O_5 was confirmed by examining the x-ray diffraction pattern.

In order to investigate the dynamics of the semiconductor-to-metal transition, we performed two types of time-resolved diffuse reflection measurements with visible light. First, to observe the dynamics between 100 fs and 1 ns, we applied a femtosecond pump-probe measurement, whose setup is shown in Fig. 1(a). As a light source, we employed a 1 kHz regenerative amplifier (Spectra Physics, Spitfire) producing 120 fs pulses at 800 nm and seeded by a mode-locked Ti:sapphire laser (Spectra Physics, TSUNAMI 3160C). The output was separated into pump and probe light by a beam splitter. Pump pulses at 800 nm wavelength, which excite *d*-*d* transitions in titanium ions [15,18], were focused on the sample with a spot diameter of 300 μm. The wavelength of the probe pulses was converted by an optical parametric amplifier (Light Conversion, TOPAS-C), and these pulses were focused on the sample with a spot diameter of 70 μm. Diffuse reflection of the probe light from the sample was collected by a photodetector and recorded by a lock-in detection system. Second, a streak camera (Hamamatsu Photonics, C5680), operated with a time resolution of about 0.7 ns, was employed to observe the dynamics longer than 1 ns, as shown in Fig. 1(b). The same femtosecond light source at 800 nm was used for pump pulses. As a probe, several semiconductor laser diodes emitting continuous waves were used depending on the probe wavelength. To avoid thermal damage to the sample, the probe light was switched on only briefly by an acoustic optic modulator that was synchronized with the pump pulses. The static diffuse reflection spectra were detected by a liquid-nitrogen-cooled charge-coupled device equipped with a monochromator, using a white halogen lamp as a light source. All the above experiments were performed at room temperature.

III. RESULTS AND DISCUSSION

A. Static diffuse reflectance spectra

In Fig. 2(a) the diffuse reflectance (DR) spectrum of the initial β phase is shown as a thick red curve. The DR spectrum of the λ phase, which is created from the β phase after pumping with 5000 shots of 8.5×10^{-7} mJ/μm^2 pulses, is also shown in Fig. 2(a) as a thin black curve. As will be discussed below, the surface of the sample is completely converted to the λ phase under these irradiation conditions. Because of the permanent phase transition, the color of the irradiated surface changes from brown to black. Since DR is basically similar to transmittance in low-absorbance regions, the decrease in the DR in Fig. 2(a) corresponds to an increase in absorbance. The absorption spectra (Kubelka-Munk spectra [33]) of the β phase and the λ phase converted from the DR spectra agree well with those in Ohkoshi *et al.* [15] (see Supplemental Material 1 [34]). We therefore confirm that the state generated by the femtosecond pulses is the λ phase. Figure 2(b) shows the difference in the DR spectrum between the β and λ phases, which is normalized by the DR spectrum of the β phase. From

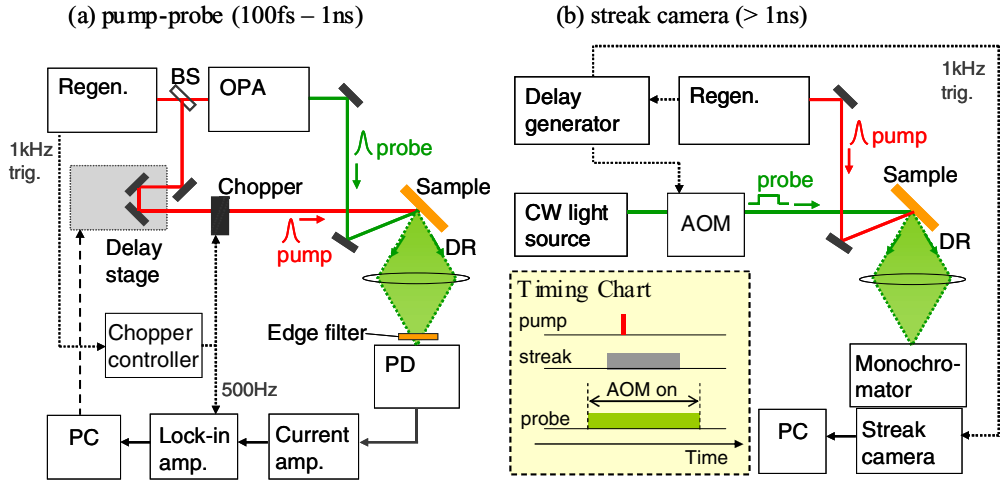

FIG. 1. (Color online) Schematics of the experimental apparatus, (a) femtosecond pump-probe measurements (100 fs–1 ns) and (b) long duration measurement (>1 ns) with a streak camera. The inset shows a timing chart for the experiment. Regen.: Ti:sapphire regenerative amplifier system, OPA: optical parametric amplifier, BS: beam splitter, DR: diffuse reflection light, PD: Si photodetector, PC: personal computer, and AOM: acoustic optic modulator.

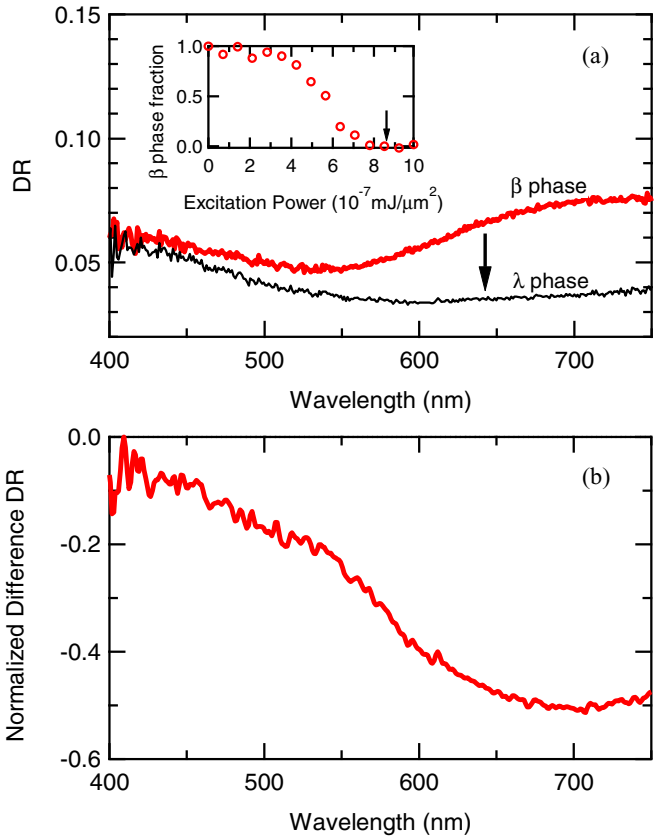

FIG. 2. (Color online) (a) Diffuse reflectance (DR) spectra of β phase (red thick curve) and λ phase (black thin curve). The λ phase was created after irradiation with 5000 pulses (800 nm, 120 fs, 500 Hz, 8.5×10^{-7} mJ/μm^2); the power of these pulses is indicated by the arrow in the inset. The inset shows the fraction of the surviving β phase versus the excitation density per pulse, which suggests the threshold behavior of the persistent phase transition. The fraction was evaluated from the intensity at 633 nm of the spectrum. (b) The difference in DR spectrum between the β phase and the λ phase, which is normalized by the DR spectrum of the β phase.

this figure we see the spectral tendency that the decrease of DR associated with the phase transition is larger at wavelengths longer than about 550 nm. In other words, the increase in absorbance at the longer wavelengths is an indication of the phase transition from β to λ phase. Hereafter, we call the difference in the DR spectrum in Fig. 2(b) as "$DR_{\beta\to\lambda}$" for simplicity.

The inset in Fig. 2(a) shows the excitation fluence dependence of the fraction of the persistent β phase after pumping by 5000 shots, which is estimated from the DR at 633 nm. By increasing the number of the incident pulses, the surviving β-phase fraction quickly saturates with less than 500 shots in these excitation conditions; the conversion yield evaluated at 5000 shots is surely regarded as a saturated value and can be used as a reliable measure of the persistent phase transition. The saturated value is determined by the excitation fluence per pulse, rather than the total deposited energy. This plot shows a clear threshold in the energy per pulse, and this is required to cause the persistent transition from β to λ phase. The fluence at the onset of the persistent transition is about 4×10^{-7} mJ/μm^2 pulse^{-1}, and the transition is completed when excited with pulses more powerful than 8×10^{-7} mJ/μm^2 pulse^{-1}. This value is consistent in order of magnitude with the previous report that applied a nanosecond green laser as the excitation source [15].

B. Time-resolved measurements

Figure 3 shows the temporal evolution of the transient diffuse reflectance (ΔDR) probed at 633 nm, after optical excitation. Here the excitation fluence was adjusted to 2×10^{-7} mJ/μm^2 pulse^{-1}, which is about half of the threshold where the persistent transition starts. The overall dynamics of the ΔDR shown in Figs. 3(a) and 3(b) can be split into the following five processes: (i) Just after excitation, the ΔDR decreases about 17% within a few hundreds of femtoseconds. (ii) Subsequently, the ΔDR increases about 7% within the next 1 ps. (iii) The ΔDR decreases again, gradually but substantially, for about 10 ps. (iv) Within the next 20 ns, the ΔDR relaxes exponentially to 10% its initial value. (v) Finally, the ΔDR attenuates nonexponentially over several hundreds of microseconds, and the sample returns to its initial state. In the inset in Fig. 3(b), where the ΔDR curve is shown in a linear time scale, the decay component with a lifetime of about 20 ns is clear. This suggests that processes (iv) and (v) should be explained by different relaxation mechanisms.

In the inset of Fig. 3(a), damped oscillations with a lifetime of several tens of picoseconds are shown. Since the period of the oscillation is proportional to the probe wavelength (see Supplemental Material 2 [34]), this component is attributed to the interference between probe pulses reflected at the front surface of the microcrystals and those reflected from the wavefront of acoustic phonon wave packets propagating into the sample. The acoustic phonon burst originates with impulsive lattice expansion, which may be associated with the phase transition. Similar periodic reflectivity modulation has often been observed in transient reflection measurements [35,36]. As the amplitude of the oscillation is less than the typical magnitude of the ΔDR, we ignore this oscillation component in the following analyses.

1. Spectral analysis

In order to understand the relaxation processes, we examined the probe wavelength dependence of the temporal behavior. Figure 4 shows four typical ΔDR spectra characterizing the relaxation stages. The corresponding stages and delay times used in Fig. 4 are noted in Fig. 3 using four capital letters, A (0 ps), B (1.3 ps), C (50 ps), and D (50 ns). First, the ΔDR spectrum at 0 ps (stage A, red filled circles) is plotted in Fig. 4. Behind it, $DR_{\beta\to\lambda}$ is plotted again with an appropriate coefficient (=0.3) and an offset for comparison (gray dotted curve). Comparing these, the spectrum at 0 ps is well represented by the spectral variation associated with the phase transition and a constant component. We ascribe the latter to Drude absorption, which is expected to be nearly flat in this wavelength range. This suggests that just after excitation, the charge ordering in the semiconductor β phase is dispersed within a few hundreds of femtoseconds, and that not only excited free carriers but also metallic λ phases are generated through the process (i). According to

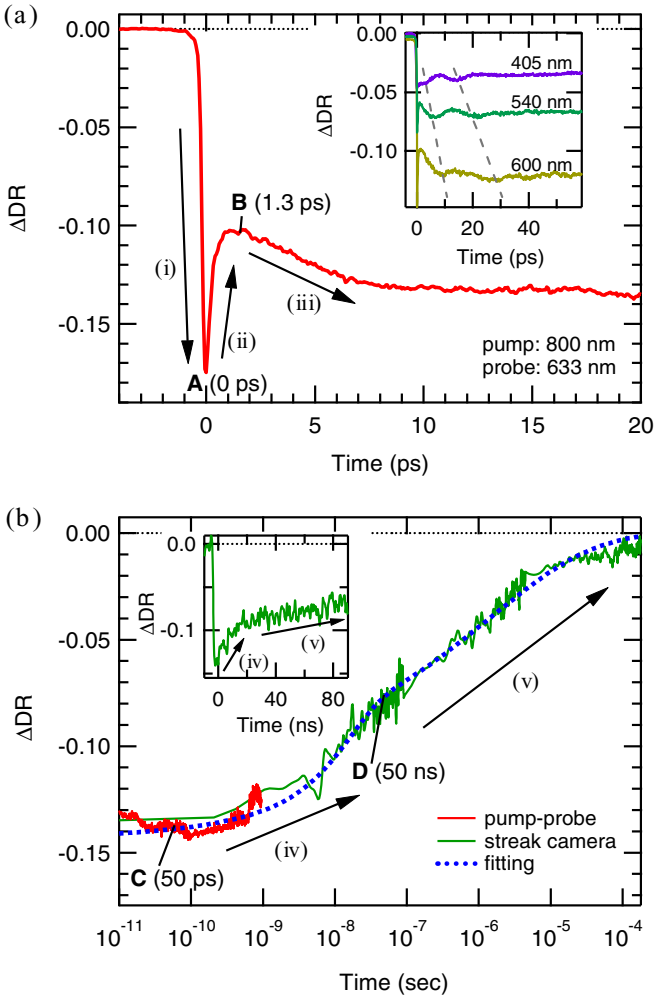

FIG. 3. (Color online) (a) Temporal evolution of the transient diffuse reflectance (ΔDR) probed at 633 nm after pumping at 800 nm. The tip of the sharp decline is referred to as the time origin (0 ps) throughout the article, though the true excitation time may be slightly earlier within temporal resolution. The inset shows the ΔDR curves probed at 405, 540, and 600 nm. The dotted lines in the inset are visual guides to show the variation of the periods in the oscillations. (b) The ΔDR curve probed at 633 nm in the range from 10 ps to 200 μs in a logarithmic scale, which is obtained by pump-probe measurement in the earlier stage (red) and by streak camera in the later stage (green). The blue dotted line is a fitting curve, which is a superposition of two decay components: an exponential function with a time constant of 20 ns and a stretched exponential function with an averaged time constant of ~20 μs and a β factor of ~0.3. See the text for details of this function. The inset shows the ΔDR curve probed by the streak camera up to 100 ns in a linear scale. The Roman indices (i)–(v) represent the characteristic five processes in the transition, while the capital letters, A (0 ps), B (1.3 ps), C (50 ps), and D (50 ns), represent the typical relaxation stages between these processes.

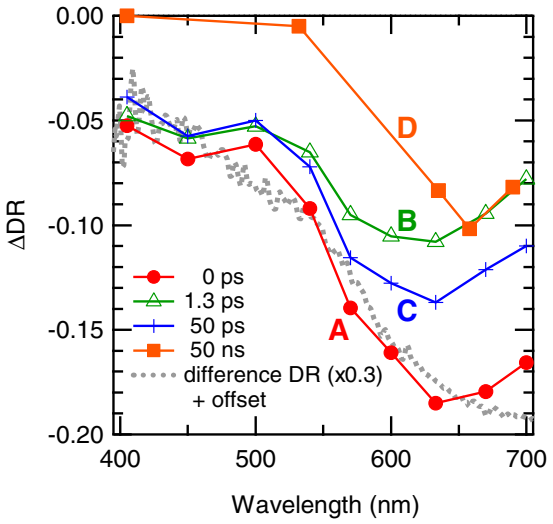

FIG. 4. (Color online) ΔDR spectra at 0 ps (red filled circles), 1.3 ps (green open triangles), 50 ps (blue crosses), and 50 ns (orange filled rectangles). Behind the spectrum at 0 ps, the difference DR spectrum ($DR_{\beta\to\lambda}$) shown in Fig. 1(b) is replotted with a coefficient of 0.3 and an offset for comparison (gray dotted curve). The capital letters A–D correspond to those defined in Fig. 3.

the coefficient (0.3) multiplied with the $DR_{\beta\to\lambda}$ in Fig. 4, the λ fraction gained here is approximately 30%. Judging from this rapid response, this phase transition is likely to be nonthermal.

Second, the ΔDR spectrum at 1.3 ps (stage B, green open triangles) is plotted in Fig. 4, which corresponds to the final state of the process (ii). By comparing this spectrum with that plotted at 0 ps, it is found that the λ component ($DR_{\beta\to\lambda}$) decreases, while the Drude component remains almost constant. This is attributed to the partial disappearance of the metastable λ phase. The ΔDR spectrum at 50 ps (stage C, blue crosses) is also plotted in Fig. 4, which corresponds to the final state of the process (iii). By comparing this spectrum with that at 1.3 ps, interestingly, we find that the λ component again increases gradually, over about 10 ps.

Third, the ΔDR spectrum at 50 ns (stage D, orange filled rectangles), which corresponds to the final state of the process (iv), is shown in Fig. 4. By comparing the spectrum with that at 50 ps, we find that only the flat component disappears. Since the residual ΔDR spectrum at 50 ns resembles the λ component, the state at 50 ns is ascribed to long-surviving metastable λ domains. From these facts, process (iv) is attributed to the extinction of the excited free carriers. As shown in the inset of Fig. 3(b), this component exponentially annihilates within 20 ns.

Based on the interpretations so far, the final process (v) over several hundreds of microseconds can be ascribed to shrinking and annihilation of the metastable λ domains. As shown in Fig. 3(b), this nonexponential decay curve can be reproduced by a stretched exponential function: $\exp[-(t/\tau)^{\beta}]$, where τ is the time constant and β is the stretching factor ($0 < \beta \leqslant 1$). From the fitting analysis between about 10^{-9} and 10^{-4} s, the average lifetime $\langle\tau\rangle$ and β are estimated to be ~20 μs and ~0.3, respectively. This result indicates that various relaxation processes with lifetimes distributed over several orders of magnitude, centered at tens of microseconds, are involved. It may also indicate wide distribution of the domain size of the metastable λ phase.

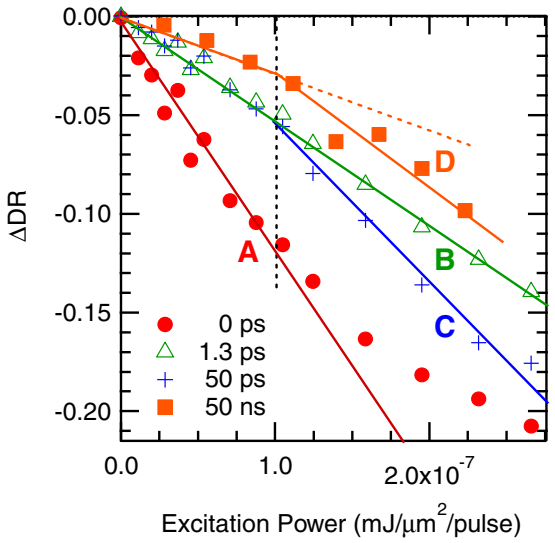

FIG. 5. (Color online) Excitation power dependence of the ΔDR probed at 633 nm at 0 ps (red filled circles), 1.3 ps (green open triangles), 50 ps (blue crosses), and 50 ns (orange filled rectangles). The capital letters A–D correspond to those in Figs. 3 and 4. The lines are visual guides for easier discrimination of the threshold behaviors.

2. *Excitation fluence dependence*

Next, we focus on the excitation fluence dependence of the ΔDR. Figure 5 shows the fluence dependence of ΔDR probed at 633 nm at stages A–D. First, we can find that the ΔDR at 0 ps (stage A, red filled circles) decreases linearly below about 1.0×10^{-7} mJ/μm^2 pulse^{-1} and starts saturating around this fluence, while the ΔDR at 1.3 ps (stage B, green open triangles) does not show such a tendency.

These fluence dependencies can be interpreted as follows. When electrons in the initial β phase are locally excited by photons, the charge ordering in the β phase is disturbed around the excited sites, and metallic λ phase domains appear. In general, domains must be larger than some critical size to survive and maintain stability; domains smaller than the critical size annihilate quickly. Therefore, in the weaker excitation range ($<1.0 \times 10^{-7}$ mJ/μm^2 pulse^{-1}), the locally generated small metallic λ-phase fragments should disappear in a short time. In addition, the amount of the transiently created λ-phase fractions is expected to be proportional to the excitation fluence.

On the other hand, the saturating behavior observed in the stronger excitation range ($>1.0 \times 10^{-7}$ mJ/μm^2 pulse^{-1}) can be explained as follows. When the already generated λ-phase domains are excited again by photons that come later, the extent of the λ phase will not increase. Consequently, as the excitation fluence increases, the quantum efficiency of nucleation decreases, resulting in the saturating behavior. Such saturation is expected to be observable when each domain is generated closely enough together to cause overlapping. Hence, the threshold fluence around 1.0×10^{-7} mJ/μm^2 pulse^{-1} can be interpreted as the critical condition where each λ-phase nucleus begins to overlap.

Second, the ΔDR at 1.3 ps decreases linearly without a threshold, while that at 50 ps (stage C, blue crosses) changes evidently in slope at 1.0×10^{-7} mJ/μm^2 pulse^{-1}. This threshold behavior suggests that the process (iii), the delayed increase of the λ-phase fraction, may involve some cooperating mechanism. We also find that the fluence dependence at 50 ns (stage D, orange filled rectangles) exhibits a similar threshold behavior. This suggests that the λ-phase domains existing at 50 ns share an origin with those found at 50 ps.

The threshold behavior at 50 ps can be understood as follows. The λ-phase fraction increases due to the growth of the λ-phase domains via cooperative interactions during process (iii). Such a domain growth process via cooperative interactions has been reported in other photoinduced phase-transition materials [37,38]. The λ-phase domains existing at 1.3 ps, which are the initial stage of the domain growth, have domain sizes large enough to survive the fast annihilation process. The response time of about 10 ps may correspond to the time required for growth to achieve a maximum. The grown domains at this stage are sufficiently large and survive for hundreds of microseconds. These interpretations that include domain growth can explain the threshold tendency observed at 50 ps.

As for explaining the slow response through processes (iii)–(v), laser heating (and cooling) can be discarded based on the following experimental facts. When ΔDR is measured at a much lower temperature of 4 K, a similar waveform to that found at room temperature is observed. Therein, the slow response ranging to several hundreds of microseconds is also observed, and the ΔDR decrease amounts to about 10% around 50 ps. On the other hand, the static DR at 633 nm is constant within a small margin of variation when the temperature is raised from 4 to 300 K. This indicates that the slow response cannot be attributed to simple laser heating.

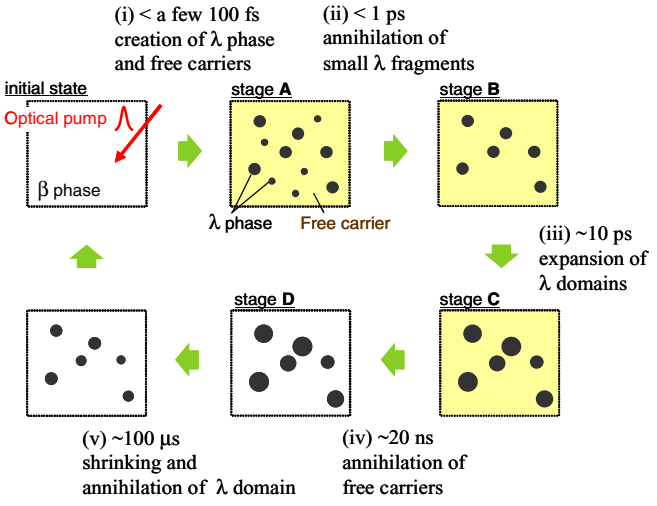

FIG. 6. (Color online) Schematic drawing of the relaxation dynamics in the case that β-Ti_3O_5 is excited below the threshold for the persistent transition. The yellow-masked background represents the excited free carriers.

C. Scenario of the semiconductor-to-metal phase transition in nanogranular Ti_3O_5

Based on the discussion so far, the photoinduced phase transition dynamics under excitation fluence that remains below the threshold is summarized in Fig. 6. (i) When the β phase is optically pumped, excited free carriers and λ-phase fractions are generated within a few hundreds of femtoseconds. (ii) The small λ-phase fragments vanish within the next 1 ps. (iii) The surviving metastable λ-phase domains expand via cooperative interactions, for about 10 ps. (iv) The excited free carriers are annihilated within 20 ns. (v) The metastable λ-phase domains shrink and annihilate within several hundreds of microseconds.

Note that in process (v) the lifetime has a wide distribution that reflects the fluctuating size of the metastable λ-phase domains. As the sample is excited with higher fluences, the average size of the λ-phase domains becomes larger and some of them will attain large enough sizes to persist, leading to a permanent phase transition. Therefore, the switching response time of the persistent phase change is also dominated by the domain expansion process, and is expected to be around 10 ps.

IV. CONCLUSION

In conclusion, we characterized the overall dynamics of the semiconductor-to-metal phase transition (β phase to λ phase) in nanogranular Ti_3O_5 by time-resolved diffuse reflection spectroscopy, over a wide range of time scales, from femtoseconds to microseconds. From the excitation fluence dependences, we found several threshold behaviors characteristic of the photoinduced phase transition. In addition, from spectral analysis, we found that the transient phase transition occurs within a few hundreds of femtoseconds and that 40% of the converted λ-phase fractions revert to β phase within 1 ps. This fast response indicates that this phase transition is a nonthermal process. Carriers are generated instantaneously and disappear within 20 ns. The delayed increase of the λ phase from 1 to 10 ps is ascribed to growth of the metallic domain. The decay components having time constants spread widely between 10^{-9} and 10^{-4} s are well represented by a stretched exponential function and ascribed to shrinking and annihilation processes of the size-distributed metallic domains. The fast onset within a few hundreds of femtoseconds and the subsequent stabilization process within 10 ps ensure the applicability of this material to ultrafast photoswitching.

In the future, the mechanism of the unique reversible phase transition in this material can be clarified by investigating the ultrafast dynamics in the inverse process (λ phase to β phase), following similar experimental techniques.

ACKNOWLEDGMENTS

This work was supported by a Grant-in-Aid for Scientific Research (A) (Grant No. 23244063) from MEXT, and A.A. was supported by a Grant-in-Aid for JSPS Fellows (Grant No. 13J10196).

[1] K. Nasu, *Relaxations of Excited States and Photo-Induced Structural Phase Transitions* (Springer, Berlin, 1997).
[2] N. Yamada, E. Ohno, K. Nishiuchi, N. Akahira, and M. Takao, J. Appl. Phys. **69**, 2849 (1991).
[3] A. V. Kolobov, P. Fons, A. I. Frenkel, A. L. Ankudinov, J. Tomonaga, and T. Uruga, Nat. Mater. **3**, 703 (2004).
[4] K. Miyano, T. Tanaka, Y. Tomioka, and Y. Tokura, Phys. Rev. Lett. **78**, 4257 (1997).
[5] M. Fiebig, K. Miyano, Y. Tomioka, and Y. Tokura, Science **280**, 1925 (1998).
[6] A. Cavalleri, C. Tóth, C. W. Siders, and J. A. Squier, Phys. Rev. Lett. **87**, 237401 (2001).
[7] S. Koshihara, Y. Tokura, T. Mitani, G. Saito, and T. Koda, Phys. Rev. B **42**, 6853 (1990).
[8] E. Collet, M. H. L. Cailleau, M. B. L. Cointe, H. Cailleau, M. Wulff, T. Luty, S. Koshihara, M. Meyer, L. Toupet, P. Rabiller, and S. Techert, Science **300**, 612 (2003).
[9] P. Gülich, A. Hauser, and H. Spiering, Angew. Chem. Int. Ed. Engl. **33**, 2024 (1994).
[10] O. Kahn and C. J. Martinez, Science **279**, 44 (1998).
[11] M. Verdaguer, Science **272**, 698 (1996).
[12] H. Tokoro, T. Matsuda, T. Nuida, Y. Moritomo, K. Ohoyama, E. D. L. Dangui, K. Boukheddaden, and S. Ohkoshi, Chem. Mater. **20**, 423 (2008).
[13] A. Asahara, M. Nakajima, R. Fukaya, H. Tokoro, S. I. Ohkoshi, and T. Suemoto, Phys. Rev. B **86**, 195138 (2012).
[14] S. Ohkoshi and H. Tokoro, Acc. Chem. Res. **45**, 1749 (2012).
[15] S. Ohkoshi, Y. Tsunobuchi, T. Matsuda, K. Hashimoto, A. Namai, F. Hakoe, and H. Tokoro, Nat. Chem. **2**, 539 (2010).
[16] R. Makiura, Y. Takabayashi, A. N. Fitch, H. Tokoro, S. Ohkoshi, and K. Prassides, Chem. Asian J. **6**, 1886 (2011).
[17] R. Liu and J. X. Shang, Model. Simul. Mater. Sci. Eng. **20**, 035020 (2012).
[18] R. Liu, J. X. Shang, and F. H. Wang, Comput. Mater. Sci. **81**, 158 (2014).
[19] O. Carp, C. L. Huisman, and A. Reller, Prog. Solid State Chem. **32**, 33 (2004).
[20] H. J. Zeiger, T. K. Cheng, E. P. Ippen, J. Vidal, G. Dresselhaus, and M. S. Dresselhaus, Phys. Rev. B **54**, 105 (1996).
[21] T. K. Cheng, L. H. Acioli, J. Vidal, H. J. Zeiger, G. Dresselhaus, M. S. Dresselhaus, and P. Ippen, Appl. Phys. Lett. **62**, 1901 (1993).
[22] M. Watanabe, M. Miyahara, and K. Tanaka, J. Phys.: Conf. Ser. **148**, 012017 (2009).
[23] M. Watanabe, W. Ueno, and T. Hayashi, J. Lumin. **122-123**, 393 (2007).
[24] M. Abbate, R. Potze, G. A. Sawatzky, C. Schlenker, H. J. Lin, L. H. Tjeng, C. T. Chen, D. Teehan, and T. S. Turner, Phys. Rev. B **51**, 10150 (1995).
[25] C. N. R. Rao, S. Ramdas, R. E. Loehman, and J. M. Hong, J. Solid State Chem. **3**, 83 (1971).
[26] M. Onoda, J. Solid State Chem. **136**, 67 (1998).
[27] L. K. Keys and L. N. Mulay, Appl. Phys. Lett. **9**, 248 (1966).

[28] J. F. Houlihan and L. N. Mulay, Phys. Status Solidi B **65**, 513 (1974).
[29] R. F. Bartholomew and D. R. Frankl, Phys. Rev. **187**, 828 (1969).
[30] J. F. Baumard, D. Panis, and A. M. Anthony, J. Solid State Chem. **20**, 43 (1977).
[31] S. Åsbrink and A. Magnéli, Acta Crystallogr. **12**, 575 (1959).
[32] W. H. Zachariasen, J. Less-Common Met. **62**, 1 (1978).
[33] P. Kubelka, J. Opt. Soc. Am. **38**, 448 (1948).
[34] See Supplemental Materials at http://link.aps.org/supplemental/10.1103/PhysRevB.90.014303 for SM1: Kuberka-Munk spectra converted from the DR spectra, and SM2: period of the phonon-induced oscillation of ΔDR depending on the probe wavelength.
[35] K. Tanimura and I. Akimoto, J. Lumin. **94-95**, 483 (2001).
[36] M. Fiebig, K. Miyano, Y. Tomioka, and Y. Tokura, Appl. Phys. B **71**, 211 (2000).
[37] H. Okamoto, Y. Ishige, S. Tanaka, H. Kishida, S. Iwai, and Y. Tokura, Phys. Rev. B **70**, 165202 (2004).
[38] M. Nakajima, N. Takubo, Z. Hiroi, Y. Ueda, and T. Suemoto, J. Lumin. **129**, 1802 (2009).